Atmos. Chem. Phys., 20, 5629–5644, 2020
https://doi.org/10.5194/acp-20-5629-2020

Atmospheric Chemistry and Physics
Open Access
EGU

Composition and volatility of secondary organic aerosol (SOA) formed from oxidation of real tree emissions compared to simplified volatile organic compound (VOC) systems

Arttu Ylisirniö[1], Angela Buchholz[1], Claudia Mohr[2,3], Zijun Li[1], Luis Barreira[1,4], Andrew Lambe[5], Celia Faiola[1,6], Eetu Kari[1,a], Taina Yli-Juuti[1], Sergey A. Nizkorodov[7], Douglas R. Worsnop[5], Annele Virtanen[1], and Siegfried Schobesberger[1]

[1]Department of Applied Physics, University of Eastern Finland, Kuopio, Finland
[2]Institute of Meteorology and Climate Research, Karlsruhe Institute of Technology, Karlsruhe, Germany
[3]Department of Environmental Science and Analytical Chemistry, Stockholm University, Stockholm, Sweden
[4]Atmospheric Composition Research, Finnish Meteorological Institute, Helsinki, Finland
[5]Center for Aerosol and Cloud Chemistry, Aerodyne Research, Inc., Billerica, MA, USA
[6]Department of Ecology and Evolutionary Biology, University of California, Irvine, Irvine, CA, USA
[7]Department of Chemistry, University of California, Irvine, Irvine, CA, USA
[a]currently at: Neste Oyj, Espoo, Finland

Correspondence: Arttu Ylisirniö (arttu.ylisirnio@uef.fi)

Received: 14 October 2019 – Discussion started: 22 October 2019
Revised: 3 February 2020 – Accepted: 5 April 2020 – Published: 13 May 2020

Abstract. Secondary organic aerosol (SOA) is an important constituent of the atmosphere where SOA particles are formed chiefly by the condensation or reactive uptake of oxidation products of volatile organic compounds (VOCs). The mass yield in SOA particle formation, as well as the chemical composition and volatility of the particles, is determined by the identity of the VOC precursor(s) and the oxidation conditions they experience. In this study, we used an oxidation flow reactor to generate biogenic SOA from the oxidation of Scots pine emissions. Mass yields, chemical composition and volatility of the SOA particles were characterized and compared with SOA particles formed from oxidation of α-pinene and from a mixture of acyclic–monocyclic sesquiterpenes (farnesenes and bisabolenes), which are significant components of the Scots pine emissions. SOA mass yields for Scots pine emissions dominated by farnesenes were lower than for α-pinene but higher than for the artificial mixture of farnesenes and bisabolenes. The reduction in the SOA yield in the farnesene- and bisabolene-dominated mixtures is due to exocyclic C =C bond scission in these acyclic–monocyclic sesquiterpenes during ozonolysis leading to smaller and generally more volatile products. SOA particles from the oxidation of Scots pine emissions had similar or lower volatility than SOA particles formed from either a single precursor or a simple mixture of VOCs. Applying physical stress to the Scots pine plants increased their monoterpene, especially monocyclic β-phellandrene, emissions, which further decreased SOA particle volatility and increased SOA mass yield. Our results highlight the need to account for the chemical complexity and structure of real-world biogenic VOC emissions and stress-induced changes to plant emissions when modelling SOA production and properties in the atmosphere. These results emphasize that a simple increase or decrease in relative monoterpene and sesquiterpene emissions should not be used as an indicator of SOA particle volatility.

1 Introduction

Secondary organic aerosol (SOA) formed from oxidation of volatile organic compounds (VOCs) comprises a large fraction of the total aerosol mass in the boreal forests of the Northern Hemisphere (Hallquist et al., 2009; Jimenez et al.,

2009; Riipinen et al., 2012). The chemical transformation of primary VOC emissions to SOA particles, which have an important climate impact (Hallquist et al., 2009), is a complicated cascade of gas-phase oxidation and multiphase ageing reactions. The physical properties of SOA are dictated by the chemical complexity of the initial VOC emissions and the oxidative conditions they experience (Glasius and Goldstein, 2016).

The formation and growth of SOA particles are often described by the absorptive partitioning of organic vapours (e.g. terpenoid oxidation products) between the gas and particle phase (Donahue et al., 2011; Pankow, 1994). The main property determining how readily organic molecules enter and stay in the particle phase is their volatility, usually expressed as saturation vapour pressure (P_{sat}) or saturation mass concentration (C^*) in air. The volatility of a specific compound is in turn determined by both its molar mass and functional group composition (Capouet and Müller, 2006; Pankow and Asher, 2008). Oxidation of a single VOC precursor produces a wide variety of semi- and low-volatility compounds, which are able to condense into the particle phase according to their C^*. The uptake of oxidation products may also involve or be facilitated by heterogeneous reactions.

In boreal forest environments, VOC emissions are dominated by monoterpenes. As the globally most important monoterpene (Spanke et al., 2001), α-pinene has been most commonly used as a model species in laboratory SOA studies. Consequently, α-pinene has been used as a proxy for all other monoterpenes in atmospheric models using its properties to describe the atmospheric oxidation and contribution to SOA particles of all other monoterpenes (Holopainen et al., 2017; Yassaa et al., 2012).

However, the VOC emission patterns of vegetation vary significantly depending on locations, environmental conditions and even genotypes of each plant. Moreover, differences in emissions can even be found between two plants of the same species with the same age located in the same environment (Bäck et al., 2012; Hakola et al., 2017; Holopainen and Gershenzon, 2010). Even though the VOC emissions from boreal forests are thought to mostly consist of monoterpenes, Hellén et al. (2018) recently showed a significant contribution of sesquiterpenes to the total VOC budget in boreal forests. This finding is in line with an earlier study by Hakola et al. (2017) that showed high emissions of sesquiterpenes measured from branch enclosures in a coniferous forest in Finland during early spring and late autumn. Mixtures of different VOCs as well as different trace gases like NO_x, CO and sulfuric acid also influence the oxidant reactivity and oxidant product distribution compared to single VOC precursor oxidation (McFiggans et al., 2019; Ng et al., 2017). These results highlight the need to use real emissions as precursors while exploring the physical and chemical properties of SOA particles.

In this study, we present results from a state-of-the-art suite of instruments used to investigate the VOC emission profile of Scots pine saplings (*Pinus sylvestris*) and subsequent SOA formation from these VOCs in an oxidation flow reactor (OFR). The central instrument in this work is a Filter Inlet for Gases and AEROsols, coupled to a high-resolution time-of-flight chemical ionization mass spectrometer (FIGAERO-CIMS; Aerodyne Research, Inc. and Tofwerk AG; Lopez-Hilfiker et al., 2014), which allowed us to characterize the composition and thermal desorption behaviour of the SOA particles. For comparison, we performed the same measurements for SOA formed from α-pinene in the same OFR. Prompted by a strong contribution of farnesenes to the emissions from our plants, we also examined SOA formation from a mixture of acyclic–monocyclic sesquiterpenes with major contributions from isomeric farnesenes and bisabolenes. This is the first volatility measurement of SOA particles formed from the oxidation of farnesene and bisabolene since earlier studies involving these sesquiterpenes have focused on the gas-phase chemistry (Kim et al., 2011; Kourtchev et al., 2009, 2012) or the chemical composition of the SOA particles (Jaoui et al., 2017). Our results show surprising impacts of the VOC mixture on the SOA particle volatility compared to SOA particles formed from a single VOC.

2 Materials and methods

2.1 VOC measurements and SOA production

We conducted experiments with SOA generated from the ozonolysis and photo-oxidation of VOCs by hydroxyl radicals (OH) in a potential aerosol mass (PAM) OFR (Kang et al., 2007; Lambe et al., 2011) in the absence of seed particles. The experimental setup is similar to that in our previous study (Buchholz et al., 2019). A schematic of the setup is shown in Fig. 1, and all experimental conditions are listed in Tables 1 and 2. We provide a very brief description of the experimental setup here, and more detailed information can be found in the Supplement (Sect. S2). A flow containing 200 to 400 ppb of the investigated VOCs was mixed with an O_3-containing flow directly before entering the OFR. With two UV lamps (254 nm), O_3 was photolysed to $O(^1D)$ which reacted with water vapour to produce OH. A wide range of OH exposure was achieved by adjusting the voltage of 254 nm UV lamps in the OFR and changing the O_3 concentration. Overall, the integrated OH exposure in the OFR ranged from approximately 6.6×10^{10} to 2.5×10^{12} molec. cm^{-3} s across all experiments as calculated according to methods described by Peng et al. (2015, 2016). This range of OH exposure corresponds to 0.5 to 19 equivalent days of atmospheric ageing at an OH concentration of 1.5×10^6 molec. cm^{-3} (Palm et al., 2016). In all experiments, the operation temperature of the OFR was 25 or 27 °C and relative humidity was between 40 % and 60 %. For the Scots pine experiments, VOCs were introduced by flushing purified air through a plant enclo-

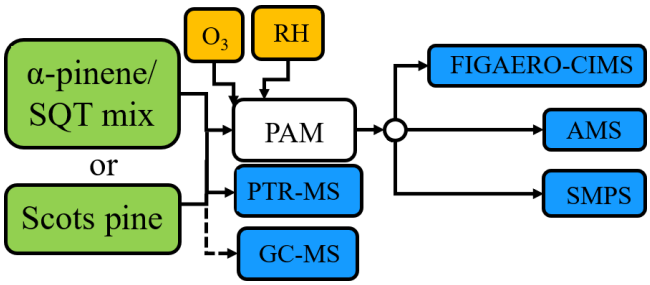

Figure 1. Measurement setup used in the experiments. Abbreviations in the picture are explained in the main text (Sect. 2), except for ozone-containing air (O_3) and humidified air (RH).

sure (Tedlar®) containing a 6-year-old Scots pine sapling. In the α-pinene (Sigma-Aldrich, 98 % purity) and sesquiterpene mix (mixture of acyclic–monocyclic sesquiterpenes, Sigma-Aldrich) experiments the VOCs were introduced into a flow of clean nitrogen by using a diffusion source or a dynamic dilution system (Kari et al., 2018). For Scots pine experiment 4, the plant was injured by making four 0.5–1 cm^2 cuts into the bark of the plant exposing resin pools and, thus, increasing the VOC emissions.

The VOC mixing ratios entering the OFR were continuously monitored using a proton-transfer-reaction time-of-flight mass spectrometer (PTR-MS; PTR-TOF 8000, IONICON Analytik Inc.) directly upstream of the OFR inlet but before the addition of O_3 to the system. All reported mixing ratios were corrected for this dilution and represent the conditions at the inlet of the OFR. In addition, to resolve the mixture of terpenoid emissions emitted by the Scots pine sapling, we collected two cartridge samples (Markes International, Inc.) at the beginning of Scots pine experiment 1 and at the end of Scots pine experiment 4 for off-line analysis using a thermal desorption gas chromatograph mass spectrometer (TD-GC-MS; TD – PerkinElmer, ATD 400, USA; GC-MS – Hewlett-Packard, GC 6890, MSD 5973, USA). The PTR-MS calibration procedure is described in Sect. S3.

The measured emission profiles from the Scots pine showed a strong contribution of α- and β-farnesene (Fig. 2), which are acyclic sesquiterpenes. Therefore, we conducted follow-up experiments under similar oxidative conditions using a commercially available mixture of acyclic–monocyclic sesquiterpenes to investigate the effect of such biogenic, unsaturated, acyclic–monocyclic VOCs on SOA properties. This sesquiterpene mixture consisted of isomers of farnesenes and bisabolene, both of which are found in the emissions of coniferous trees as well as the emissions of Scots pines in this study (Blande et al., 2009; Holopainen and Gershenzon, 2010). For a detailed description of the mixture see Tables S1 and Fig. S1 in the Supplement. For those follow-up experiments, a nominally identical OFR was used (PAM 2). However, to recreate the same OH exposure and particle composition (as characterized by the particle oxidation ratio; see below), a different combination of light intensity, residence time, and O_3 concentration was necessary in the follow-up experiments. Thus, the results are presented separately and marked PAM 1 or PAM 2.

2.2 SOA particles characterization

SOA particles were examined with a suite of instruments sampling from the outlet of the OFR: a high-resolution time-of-flight aerosol mass spectrometer (AMS; Aerodyne Research, Inc.), a scanning mobility particle sizer (SMPS; TSI Inc., Model 3082 with TSI Model 3775 condensation particle counter) and a FIGAERO-CIMS using the iodide ionization scheme (Lee et al., 2014). The AMS and SMPS were used to continuously monitor the output SOA particle mass and size distribution from the OFR to determine the point when the particle concentrations and distributions had stabilized for a given OFR condition. Then the filter collection for FIGAERO-CIMS was started so that only steady-state SOA was sampled. More information about these other instruments is given in Sect. S4.

The FIGAERO-CIMS was used to characterize the volatility and chemical composition of the SOA particles for those organic compounds sensitive to iodide cluster ionization. Briefly, in the ionization region of the instrument, operated at 100 mbar pressure, an I^- anion preferably clusters with a neutral molecule M which contains hydroxy, hydroperoxy, carboxyl or peroxycarboxyl groups in their structure. The neutral molecule is then observed as $[M+I]^-$ in the mass spectrometer (Iyer et al., 2017; Lee et al., 2014). In the presence of water, collision of an $[H_2O+I]^-$ anion cluster with M may produce the same result. In some cases, the $[M+I]^-$ cluster breaks apart leading to deprotonation of the neutral molecule, which is then observed as $[M-H]^-$, and possibly to other ion fragments. This phenomenon has also been observed in earlier studies (e.g. Lee et al., 2014). For the further analysis, we assume that deprotonation is the only mechanism of declustering, as it is one known to potentially follow from even relatively soft collisions. Additional declustering may happen by more energetic collisions in the lower-pressure regions of the mass spectrometer (Passananti et al., 2019).

In the FIGAERO inlet, the aerosol particles were sampled through 2 m stainless steel tubing (outer diameter 6 mm) onto a Teflon filter (Zefluor 2 µm polytetrafluoroethylene (PTFE) membrane filter, Pall Corp.) for 2–5 min with a collection flow of 2 L min^{-1}. The particles were then evaporated into the instrument with a gradually heated nitrogen flow with a heating rate of 11.6 K min^{-1} heated up to 200 °C over a period of 20 min and then kept at 200 °C for an additional 10 min to evaporate any residual compounds. This results in temperature-dependent ion signals for each observed mass spectrum peak (thermograms) that can be related to the volatility of the collected organic compounds (Lopez-Hilfiker et al., 2014, 2015). In this study, two

Table 1. List of different Scots pine experiments with corresponding PAM 1 reactor conditions. Monoterpenes are referred to as MT and sesquiterpenes as SQT. Collected mass is estimated from SMPS data assuming a particle density of 1.3 g cm^{-3}.

Experiment	Scots pine 1	Scots pine 2	Scots pine 3	Scots pine 4
VOC mixing ratio (ppb from PTR-ToF-MS)	MT: 125 ± 1 SQT: 179 ± 1 Sum: 304 ± 2	MT: 213 ± 14 SQT: 179 ± 1 Sum: 391 ± 14	MT: 127 ± 4 SQT: 151 ± 1 Sum: 278 ± 4	MT: 153 ± 3 SQT: 66 ± 2 Sum: 218 ± 3
SQT / MT ratio (by molar ratio)	1.43	0.85	1.2	0.4
SQT / MT ratio (by mass ratio)	2.15	1.26	1.78	0.65
OH exposure (molecules cm^{-3}s)	6.41×10^{11}	6.49×10^{11}	6.45×10^{11}	7.31×10^{11}
PAM residence time (s)	300	300	300	300
O_3 mixing ratio (ppm)	4.9	5	5	5.6
Collected mass on FIGAERO filter (ng)	1000	1200	1300	1000

Table 2. List of different α-pinene and sesquiterpene experiments with corresponding PAM reactor conditions. Collected mass is estimated from SMPS data assuming a particle density of 1.3 g cm^{-3}.

	PAM 1			PAM 2	
Experiment	α-pinene low exposure	α-pinene medium exposure	α-pinene high exposure	Sesquiterpene mixture	α-pinene reference
VOC mixing ratio (ppb from PTR-ToF-MS)	199 ± 2	198 ± 2	196 ± 2	327 ± 5	270 ± 10
OH exposure (molecules cm^{-3} s)	2.54×10^{11}	6.85×10^{11}	2.45×10^{12}	8.2×10^{10}	2.6×10^{11}
PAM residence time (s)	120	120	120	160	160
O_3 mixing ratio (ppm)	6.6	25	25	13.3	13.2
Collected mass (ng)	960	880	1350	550	925

slightly different FIGAERO inlets were used: one in conjunction with the initial experiments using the PAM 1 reactor (FIGAERO 1) and the other when using the PAM 2 reactor later on (FIGAERO 2). The CIMSs themselves were nominally identical, and both of the FIGAERO inlets followed the identical principles and were operated identically. The differences were in the detailed design of the FIGAERO inlets, e.g. the shape of the filter collection tray and exact positioning of the temperature sensor. These changes led to apparent shifts in the measured thermograms. To account for this, we performed instrument-specific calibrations for both FIGAERO inlets, which are described in more detail in Sect. 2.2.2.

A blank measurement, meaning a measurement with no particles collected on the filter, was performed before each measurement to make sure the filter was clear of residual compounds and to determine any instrument artefacts. To ensure that the filter did not contain any particles, collection flow leading to the filter was shut down between actual measurements. These blank measurements were also considered in the data analysis. The relatively high collected particle mass loading (between 500 and 1350 ng) on the filter ensured that the majority of the signal came from the evaporating SOA particles and that the instrument background and artefacts were neglectable. The FIGAERO filter was also visually inspected daily and replaced when needed.

2.2.1 FIGAERO-CIMS data analysis

The FIGAERO-CIMS data were analysed with the MATLAB-based tofTools (Junninen et al., 2010) software, including the identification of elemental compositions (creation of peak lists) based on the high-resolution (HR) peak fitting with mass accuracy of 5 ppm. All data shown here are based on the HR fitting of the mass spectra using peak lists covering the full spectra. The presented mass values are those of the neutral composition (M), derived by subtracting the molecular mass of I^- when $[M+I]^-$ was observed or by adding the molecular mass of H when $[M-H]^-$ was observed. The assigned formulas were constrained to contain only C, H and O elements; any signal peak appearing to contain other elements was considered background and excluded from further analysis. This background consisted mostly of fluorine-containing compounds, which we assume to originate from the FIGAERO inlet manifold or the collection filter, both of which are made of PTFE.

2.2.2 T_{max}-to-saturation-concentration calculations

Typically, the thermograms collected from the heat-induced SOA evaporation in the FIGAERO filter comprise a clearly defined peak, i.e. a temperature at which the largest signal is observed (T_{max}). It has been shown that T_{max} correlates with

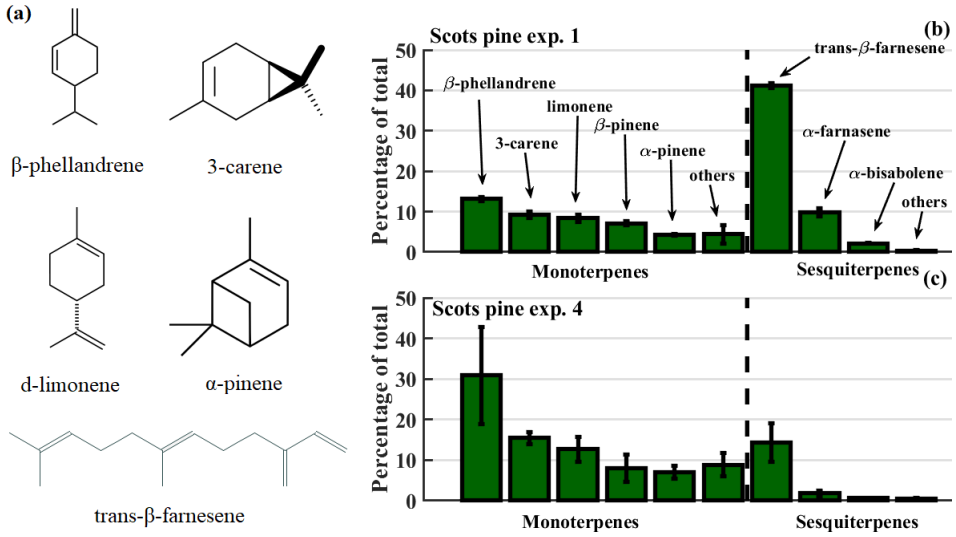

Figure 2. Panel **(a)** shows the structures of the most abundant monoterpenes and sesquiterpenes in Scots pine emissions, as measured with a TD-GC-MS. Relative mass concentrations of each compound are shown for Scots pine experiments 1 **(b)** and 4 **(c)**, the latter following deliberate damage to the plant's stem. The whiskers show the standard deviation of the measurements.

the volatility of the desorbing organic compound, typically expressed as saturation concentration C^*, at least for systems with a limited number of compounds (Bannan et al., 2019; Lopez-Hilfiker et al., 2014). We determined the relationship between T_{max} and C^* for both FIGAERO inlets independently, based on the results of calibration experiments using a series of polyethylene glycols (PEGs) with known saturation pressures P_{sat} (Pa) at reference temperature of 298.15 K (Bannan et al., 2019; Krieger et al., 2018). All reported C^* and P_{sat} values are thus contrasted with this temperature. The calibration method and resulting parameters are described in the Supplement Sect. S5.

2.2.3 SOA yield calculations and theoretical yields

From the amount of consumed precursor VOC (ΔVOC) and the condensed (i.e. particulate) organic mass (ΔC_{OA}) one can calculate the effective SOA mass yield Y by

$$Y = \frac{\Delta C_{OA}}{\Delta \mathrm{VOC}_{MT+SQT}}. \quad (1)$$

The subscripts here refer to monoterpenes (MT) and sesquiterpenes (SQT), which were the dominant contributors to SOA formation in these experiments. The $\Delta \mathrm{VOC}_{MT+SQT}$ ($\mu g\,m^{-3}$) was calculated from the difference in the total concentrations of monoterpenes and sesquiterpenes entering the OFR and the VOC concentration exiting the OFR, which was quantified by the PTR-MS. Measured mixing ratios of both MT and SQT exiting the OFR were < 1 ppb. The condensed organic mass ΔC_{OA} ($\mu g\,m^{-3}$) was monitored using the SMPS number size distribution and assuming a particle density of $1.3\,g\,cm^{-3}$ for all measurements (Faiola et al., 2018). No wall-loss correction was applied to the VOC and particle measurements. However, because the VOC measurement was made almost immediately before the inlet of the OFR and formed SOA size distribution was roughly identical between different experiments, we assume that possible sampling line wall losses have a minor impact on our SOA yield calculations.

The SOA yield can also be expressed using the approach of Odum et al. (1996), which allows for formally breaking down SOA formation into the contribution of several VOC species:

$$Y = \Delta C_{OA} \sum_i \frac{\alpha_i K_i}{1 + K_i \Delta C_{OA}}, \quad (2)$$

where α_i is a proportionality constant relating the amount of reacted VOC (precursor) to the total concentration of species i (oxidation product) and K_i is the partitioning coefficient for species i. We use a two-product version of Eq. (2), which is common in modelling applications.

2.3 Scots pine sapling treatment

Due to scheduling constraints, the experiments were conducted in early autumn outside of the most active emission time for Scots pines. To circumvent this, a Scots pine sapling (6 years old) was stored in a cold room throughout the summer to maintain winter dormancy. It was removed from the cold room ~ 1 month before experiments to initiate spring phenology and metabolism – the time of year when Scots pines are active with new shoot growth. At least 24 h before the SOA experiments, the sapling was transported to the laboratory and a dynamic Teflon plant enclosure was installed around the plant foliage. The Teflon enclosure (custom-built; Jensen Inert Products, Inc.) was secured to the plant stem

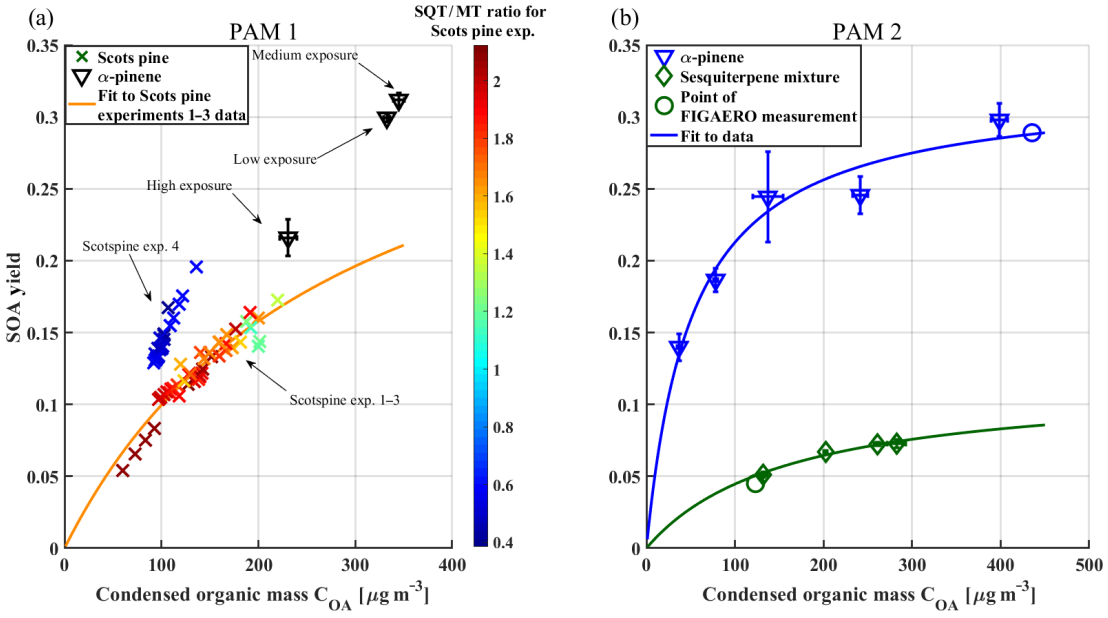

Figure 3. (a) SOA yield vs. condensed organic mass (C_{oa}) from Scots pine and α-pinene experiments. Each point represents a single SMPS scan. In these cases, error bars are omitted for clarity. The colour scale of the Scots pine experiment results corresponds to the sesquiterpene-to-monoterpene (SQT / MT) ratio by mass ratio (crosses; showing all yield measurements, reflecting the variability in plant emission rates). Each α-pinene experiment is averaged to one point (black triangles) and labelled. Error bars shown are standard deviations of multiple scans. The orange curve is fit with Eq. (2) to the Scots pine experiments 1–3 (SQT / MT > 1) with the following fit parameters: $\alpha_1 = 0.3783$, $K_1 = 0.0035$, $\alpha_2 = 0.0029$ and $K_2 = 0.0035$. **(b)** α-pinene reference and sesquiterpene mixture SOA yields versus C_{OA} and Odum fits to both datasets. The fit parameters are $\alpha_1 = 0.3219$ and $K_1 = 0.0195$ for α-pinene and $\alpha_1 = 0.1164$ and $K_1 = 0.0062$ for the sesquiterpene mixture. Circles show the points of FIGAERO measurements. Titles PAM 1 **(a)** and PAM 2 **(b)** refer to different PAM reactors used in the experiments.

with two cable ties. The plant enclosure was flushed with 5 L min^{-1} purified compressed air and operated under positive pressure to push enclosure air into the flow reactor through perfluoroalkoxy alkane tubing. The flow of plant enclosure air into the OFR was regularly measured in-line and maintained at 1.7–1.9 L min^{-1}. Three LED lamps were placed around the plant to provide photosynthetically active radiation (PAR) similar to ambient levels in Finland.

3 Results and discussion

3.1 Scots pine emission patterns

The VOC emissions from the Scots pine sapling were mainly composed of monoterpenes and sesquiterpenes. The emissions were monitored on-line with the PTR-MS and off-line with the TD-GC-MS, the latter allowing us to better speciate the VOCs by distinguishing between isomers. In Fig. 2 we show the chemical structures of the most abundant compounds (see Table S2 for full list), along with the relative concentrations of the individual monoterpenes and sesquiterpenes, as measured by the TD-GC-MS.

Among the monoterpenes, β-phellandrene had the highest concentration, followed by 3-carene, d-limonene, and β- and α-pinene, in that order. These five monoterpenes accounted for 90 % of all monoterpenes in all experiments. Among the sesquiterpenes, β- and α-farnesene and α-bisabolene were the most abundant species, accounting for about 95 % of all sesquiterpenes. All sesquiterpenes combined accounted for 55 %–70 % of the total VOC mass concentration in the Scots pine experiments 1–3 and for 40 % in Scots pine experiment 4, based on PTR-MS measurements. Relating these results to the ambient pine emission characterizations by Bäck et al. (2012), our Scots pine sapling may be classified as a 3-carene chemotype, due to the higher emission of 3-carene. The fraction of sesquiterpene emissions in our study was considerably higher than expected from the ambient pine emission measurements of the SQT / MT ratio of typically ~ 0.1 by mixing ratio (Hellén et al., 2018). The used Scots pine sapling was infested with herbivores, creating biotic stress for the plant and changing the VOC emission pattern. This type of biotic stress is natural, especially in a changing climate where insect outbreaks are predicted to become more frequent (Bale et al., 2002; Jactel et al., 2019).

During Scots pine experiments 1–3, the VOC levels slowly decreased over time. Therefore, after the end of Scots pine experiment 3, we made four 0.5–1 cm^2 cuts to the Scots pine sapling's stem, with the goal of increasing VOC emissions

to continue the production of sufficient SOA. The wounds exposed plant resin pools in the stem and increased the measured monoterpene concentrations compared to pre-cutting concentrations by roughly doubling them. Sesquiterpene concentrations, however, were not significantly affected. The compound that increased most was β-phellandrene, emissions of which had also been shown to increase with bark beetle infestation damage (Amin et al., 2012; Faiola et al., 2018). Such damage essentially consists of cuts into the stem as the bark beetle feeds on the plant; hence that observation is consistent with expectations.

3.2 SOA mass yields

In Fig. 3, we plot SOA yields against condensed organic mass C_{OA} from each experiment, split into two panels according to which of the two PAM reactors was used (Fig. 3a, PAM 1; Fig. 3b, PAM 2). Note that a similar organic mass range was covered in all experiments.

Scots pine experiments 1–3 featured sesquiterpene-to-monoterpene ratios (SQT / MT) by mass ratio between 1.2 and 2 (colour-coding in Fig. 3a). The SOA yields obtained during these experiments are consistent with each other in the sense that all the data points are well described by the same two-product model (orange line). The SOA yields resulting from Scots pine experiment 4 are about 30 % larger, even though SQT / MT was substantially smaller than in experiments 1–3. An earlier study by Faiola et al. (2018) reported a positive correlation with SOA yield and the SQT / MT ratio of VOCs measured from Scots pine seedlings in a flow tube experiment similar to our study.

To understand the unexpected suppression of SOA yield at higher relative concentrations of SQT, we also measured SOA yields for a synthetic sesquiterpene mixture containing isomers of farnesene and bisabolene. A different PAM reactor had to be used; therefore we compare those results to a reference α-pinene experiment using the same reactor (Fig. 3b). The ingoing VOC concentration was varied for both precursors, and yield measurements were conducted in order to cover the C_{OA} range of the Scots pine experiments. A single FIGAERO measurement was made for both precursors, and the corresponding sampling conditions are marked with circles in Fig. 3b. The comparison shows a clearly lower yield for the sesquiterpene mixture than for α-pinene, which is in line with results shown in Fig. 3a. Note that the medium- and low-exposure α-pinene measurements in PAM 1 show similar yield values to those in the reference experiment in PAM 2, but the yield of the high-exposure experiment is significantly lower. This is consistent with the extensive fragmentation expected inside the PAM reactor under strong oxidative conditions, which reduces the effective SOA yield (Lambe et al., 2012).

We conclude that the increase in SOA yield in Scots pine experiment 4, compared to Scots pine experiments 1–3, is likely due to the large relative increase in emitted monoterpenes, especially β-phellandrene, caused by cutting the sapling (Fig. 2). We surmise that β-phellandrene must have a high SOA yield, possibly comparable to that of d-limonene, which has been reported in the range of 50 %–60 % (Berg et al., 2013; Lee et al., 2006; Surratt et al., 2008) and which shares some structural similarity with β-phellandrene (Fig. 2). Mackenzie-Rae et al. (2017) measured SOA yields of α-phellandrene, an isomer of β-phellandrene with an endocyclic C=C bond, and found the SOA yield to be around twice that of α-pinene, reaching up to 100 %. While those yield numbers are not directly comparable to our results, they qualitatively indicate that SOA yields from monocyclic monoterpenes, with endocyclic C=C bonds, could be higher than those from the more commonly studied bicyclic monoterpenes, such as α-pinene.

It is instructive to compare our SOA yield results to results of earlier experiments that used (stressed) Scots pines. Faiola et al. (2018) studied SOA formation from emissions of herbivore-stressed Scots pines in a custom-made OFR where the main SQT type was β-caryophyllene. There the increasing SOA yields with increasing SQT contribution to the precursor mix were explained by the much higher SOA yield of β-caryophyllene (Faiola et al., 2018). In chamber studies with emissions of aphid-stressed Scots pines in which farnesenes were the dominant SQT species, SOA yields decreased with increasing SQT contribution for ozonolysis reaction while no change was observed for pure OH reaction experiments (Faiola et al., 2019). In our experiments in the PAM reactor, the ratio between O_3 and OH exposure was in the range of 10^5 which is comparable to ambient levels (Kang et al., 2007). Due to their very fast reaction with O_3, more than 80 % of any SQT are expected to react with O_3 under these conditions (calculated with methods described by Peng et al., 2015, 2016). Thus, the SOA yield should decrease with increasing amounts of farnesene as described for the ozonolysis reaction pathway in Faiola et al. (2019).

The reason for this different behaviour of the two SQT types is based on their molecular structure. β-caryophyllene is a bicyclic compound with one endo- and one exocyclic C=C bond, whereas farnesene isomers are acyclic compounds with four C=C bonds. In the (photo-)oxidation process, both ozone and OH break the C=C bonds and thus the carbon backbone of farnesene into small fragments. Just a single oxidation step decreases the number of carbons from 15 to 5–12 (Kourtchev et al., 2009, 2012). In the case of the bicyclic β-caryophyllene, such fragmentation is expected to be much less prominent (Jaoui et al., 2003, 2013).

There may be further interactions between the small, most likely volatile, farnesene reaction products and the other oxidation products, suppressing the particle formation further as recently described by McFiggans et al. (2019).

3.3 SOA composition

Figure 4 shows mass spectra integrated over the heating period of FIGAERO-CIMS measurements normalized to the maximum signal and molecular mass adjusted to neutral compositions (Sect. 2.2.1). The results are grouped into two portions as two different PAM reactors and FIGAERO inlets were used in the measurements (Sect. 2.2). The α-pinene measurements (Fig. 4, top row) show a decrease in the average molecular weight with increasing OH exposure, which is consistent with the decrease in SOA mass yields as a function of OH exposure observed in Fig. 3 and also observed in an earlier study (Hall et al., 2013).

The distribution of molecular weights of compounds in the sesquiterpene mixture SOA particles (Fig. 4, right) shifted more towards smaller molecular masses than it did in any other experiment. We explain this by the acyclic molecular structure of the sesquiterpene compounds leading to their more efficient splitting into smaller products (fragmentation) during oxidation (see Sect. 3.2). The α-pinene reference spectra differ slightly from other α-pinene measurements, even though OH exposure falls between medium and high exposure (Table 2).

The difference might be due to the different residence time inside the PAM reactor (120 vs. 160 s) or to the higher mixing ratio of VOCs in the experiment performed with the PAM 2 reactor. The FIGAERO mass spectra distribution of SOA formed from the Scots pine emissions had the most similarities to high-exposure α-pinene SOA, with almost all compounds appearing within a single mode, roughly centred on the monomer mode of the other α-pinene experiments.

Table 3 shows the average carbon oxidation states (OS_C; Kroll et al., 2011) and the average O : C ratio, calculated from both AMS and FIGAERO data. The average chemical composition is also calculated from FIGAERO data. All FIGAERO data values are weighted averages, using the integrated signal strength of each ion thermogram as weights. The range of values calculated from the FIGAERO data represents the spread of different compounds in the mass spectrum, which we will investigate below.

In the α-pinene experiments with PAM 1, the average O : C ratio and OS_C increase with the increasing oxidative strength as expected while the average carbon chain length decreases. In terms of the average O : C ratio or OS_C, the Scots pine experiments most closely correspond to the medium exposure α-pinene experiment. Interestingly, all Scots pine experiments appear broadly similar from this viewpoint, even though experiment 4 is associated with emissions dominated by monoterpenes (i.e. much smaller SQT / MT ratio) and clearly higher SOA yields (Figs. 2 and 3a). However, the Scots pine SOA particles differ from each other and from other experiments in other ways, as we will see in Sect. 3.4.

3.4 SOA volatility

In Fig. 5, we show normalized "sum" thermograms, calculated by summing up the thermograms from all ions that contain only C, H and O atoms. With these sum thermograms, the average thermal desorption behaviour can be compared across multiple experiments. While viewing the thermograms, it is important to know that the thermal decomposition during the aerosol desorption from the FIGAERO filter often manifests as signal at relatively high desorption temperatures, which may appear as shoulders to the main peak, but it can appear as simple peaks as well (e.g. Lopez-Hilfiker et al., 2015; Schobesberger et al., 2018).

For the α-pinene experiments, the sum thermograms reveal a clear increase in T_{max} (dashed vertical lines in Fig. 5a) with increasing oxidative exposure. As we have shown above, this change is concurrent with a decrease in molecular size and an increase in average O : C-ratio (Fig. 4 and Table 3). Together, these observations imply that α-pinene photo-oxidation successively forms compounds with lower volatility. Evidently, the oxidation reactions are both fragmenting, which generally increases volatility, as well as functionalizing, which generally decreases volatility (Capouet and Müller, 2006; Pankow and Asher, 2008). The clearly increasing T_{max} values observed with FIGAERO suggests a net decrease in volatility due to these processes overall, for the condensed-phase constituents, consistent with the results of isothermal evaporation experiments performed using the same (but size-selected) aerosol (Buchholz et al., 2019).

The sum thermograms for the Scots pine experiments gradually shift towards yet higher desorption temperatures (Fig. 5b); all their T_{max} values are higher than those of any of the α-pinene experiments (Fig. 5a). In particular, SOA particles from Scots pine experiment 4 are the most resistant to thermal desorption. That experiment was also the only one with plant emissions clearly dominated by monoterpenes (Fig. 2), specifically with β-phellandrene being the most abundant, which we associated above with relatively high observed SOA yields (Sect. 3.1). That specific VOC mix in Scots pine experiment 4 is unique within our study here. It is plausible that this mix is also directly responsible for producing SOA with the lowest effective C^* as suggested by the results of our FIGAERO measurements (Fig. 5, as well as our more detailed discussion below).

We suggest that the increased desorption temperatures for the Scots pine experiments 1–3 relative to the α-pinene experiments are due to the large contribution of acyclic sesquiterpenes (in particular farnesenes, Fig. 2) to the plant emissions in those experiments. We tested this hypothesis via our follow-up experiments using the PAM 2 reactor and FIGAERO 2 (Fig. 5c). These experiments yielded sum thermograms for SOA particles formed from the farnesene-dominated sesquiterpene mixture, and those from α-pinene using the same setup, for reference. The reference α-pinene SOA particles had a $\langle O:C\rangle_{AMS}$ of 0.77, similar to those

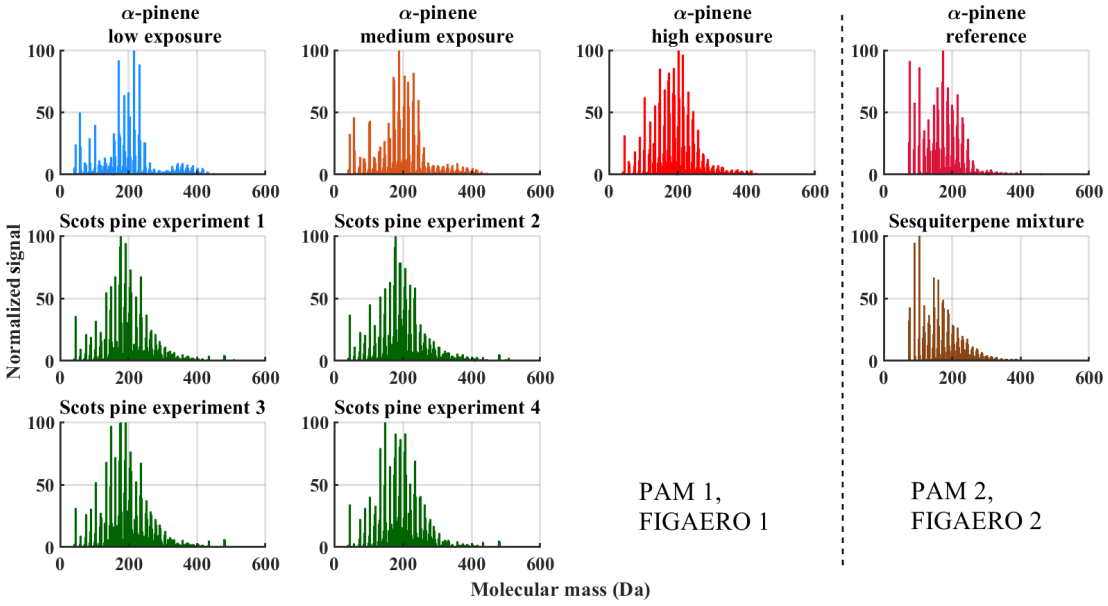

Figure 4. Mass spectra integrated over the whole FIGAERO desorption cycle for each experiment. Each spectrum is normalized to the peak height of the most abundant ion.

Table 3. Average O : C ratio, OS_C and chemical composition from each experiment calculated from AMS and FIGAERO data. Values calculated from FIGAERO are weighted by the integrated signal strength. All FIGAERO data are shown with standard deviation to highlight the spread of different compositions in the mass spectrum.

Experiment	⟨O : C⟩ AMS	⟨O : C⟩FIGAERO	⟨OS_C⟩AMS	⟨OS_C⟩FIGAERO	⟨$C_xH_yO_z$⟩
α-pinene low exposure	0.53	0.65 ± 0.28	−0.46	-0.3 ± 0.56	$C_{9\pm4}H_{14.2\pm4}O_{5.4\pm4}$
α-pinene medium exposure	0.69	0.75 ± 0.3	−0.05	0.02 ± 0.65	$C_{8.3\pm3.5}H_{12.1\pm3.5}O_{5.7\pm3.5}$
α-pinene high exposure	0.96	0.9 ± 0.33	0.63	0.47 ± 0.73	$C_{7.5\pm3}H_{9.9\pm4.5}O_{6\pm1.9}$
Scots pine experiment 1	0.85	0.79 ± 0.43	0.37	0.02 ± 1.1	$C_{8.5\pm4}H_{13.6\pm8}O_{5.4\pm2}$
Scots pine experiment 2	0.89	0.77 ± 0.42	0.43	-0.04 ± 1.1	$C_{8.4\pm4}H_{13.5\pm8.3}O_{5.4\pm2.1}$
Scots pine experiment 3	0.9	0.79 ± 0.43	0.55	0.02 ± 1.1	$C_{8.7\pm4}H_{14\pm7.9}O_{5.4\pm2.1}$
Scots pine experiment 4	1	0.81 ± 0.43	0.75	0.06 ± 1.1	$C_{8.2\pm3.7}H_{13.1\pm7.5}O_{5.3\pm2}$
Sesquiterpene mixture	0.82	0.89 ± 0.37	0.26	0.47 ± 0.83	$C_{7.5\pm3.7}H_{9.7\pm5.1}O_{5.6\pm1.8}$
α-pinene reference	0.77	0.82 ± 0.33	0.06	0.28 ± 0.71	$C_{7.4\pm3}H_{10\pm4.4}O_{5.3\pm1.5}$

in the medium- and high-exposure α-pinene case. Indeed, the sum thermogram T_{max} value for the sesquiterpene mix case is about 10 °C higher than for the reference α-pinene case, confirming that the strong contribution of farnesene and sesquiterpenes with similar structures leads to the effectively lower-volatility aerosol particles (as measured by FIGAERO) in the Scots pine experiments 1–3 compared to α-pinene SOA particles. As mentioned earlier (Sect. 2.2), a quantitative comparison of thermograms between Fig. 5c and a–b, including comparison of T_{max} values, is not straightforward, due to the differences in the respective experimental setups. However, we will deal with this issue below.

We provide a more extended discussion of our examination of SOA volatilities, which includes graphical depictions of the individual ion thermograms, in the Supplement (Sect. S6). When looking at individual experiments, the T_{max} value for each ion broadly depends on the molecular weight of the ion, as expected. However this dependency seems to differ in scale between experiments. Some signatures of thermal decomposition are visible as well, but overall this appears to play a minor role, with very small effects on the thermogram in most individual ion cases.

The resistance to thermal desorption at each unit mass appears to increase with increasing strength of oxidation in the α-pinene experiments, as is observed in the sum thermograms (Fig. 5), while the contribution of thermal decomposition appears to increase concurrently. The Scots pine experiments show similar effects between Scots pine experiments 1–4, but the change is not as pronounced as with α-pinene experiments and cannot be as clearly attributed to a single factor such as oxidative strength.

Previous studies have indicated that the T_{max} value of individual thermograms largely remains controlled by the C^* of the respective compound, even when a substantial frac-

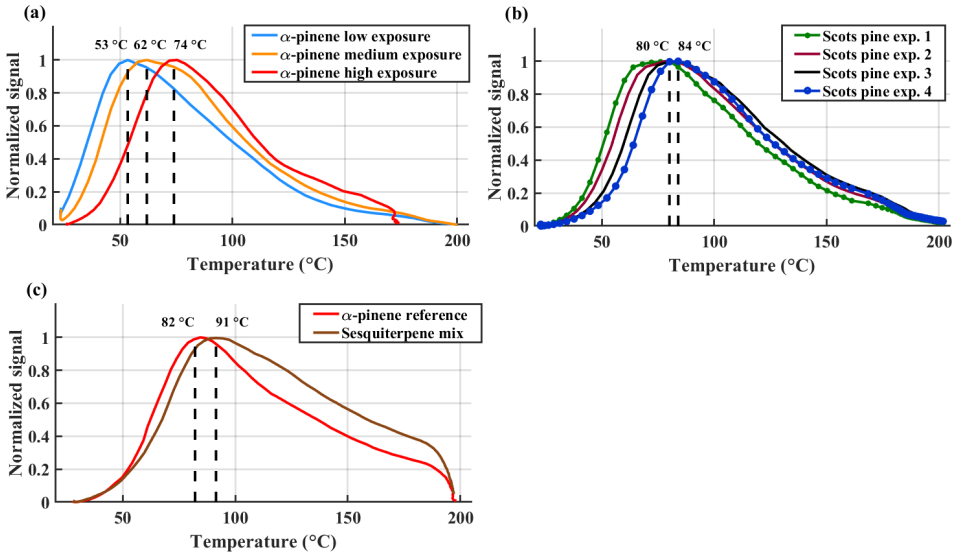

Figure 5. Normalized sum thermograms (all observed ions containing C, H and O atoms) from **(a)** α-pinene experiments, **(b)** Scots pine experiments 1–4 and **(c)** sesquiterpene mixture experiment together with reference α-pinene experiment. T_{max} values of the sum thermograms are shown with dashed lines. In panel **(b)** only the T_{max} values of Scots pine experiment 1 and Scots pine experiment 4 are shown for clarity.

tion of the signal is the result of thermal decomposition of different, larger structures (e.g. Schobesberger et al., 2018). The reason is that this decomposition typically occurs only at temperatures sufficiently higher than the desorption temperatures for most compounds. Measured T_{max} values can therefore be used as a fairly robust estimation of C^* of the respective composition. Thus, we performed calibration experiments, in order to establish the T_{max}–C^* relationship for both FIGAERO inlets used in this study (see Sect. S5), and accordingly derived C^* for each measured organic composition from its respective T_{max} value. Note that in cases where thermogram peaks are affected by thermal decomposition (which we determined play a relatively minor role in this study), we implicitly assign upper-limit C^* values. We also note that relatively high collected aerosol mass (on the order of 1 µg) might induce so-called matrix effects in the evaporation process (Huang et al., 2018), which might in turn shift the observed T_{max} to higher temperatures and could consequently lead to a slight systematic underestimation of C^*.

The results from the T_{max} to C^* conversion are shown in Figs. 6 and 7, summarizing them as volatility basis set (VBS) bins of 1 order of magnitude of C^*, as defined by Donahue et al. (2011; SVOC is semi-volatile organic compound, green volatility range; LVOC is low-volatility organic compound, red volatility range; ELVOC is extremely low volatility organic compound, grey volatility range). These VBS distributions represent only the compounds found in the particle phase. Note that having translated from T_{max} to C^* using the instrument-specific calibration parameters, all results become comparable to each other. Also note that the abundance of SVOCs might generally be underestimated due to the fast evaporation of particulate matter during collection to the FIGAERO filter and switching from collection phase to desorption phase.

A clear shift from higher to lower volatility for α-pinene SOA is observed with increasing OH exposure (Fig. 6). This shift manifests itself in the reduction in SVOC while the amount of LVOC increases. For sesquiterpene mixture SOA particles, a major part of the observed compounds falls into the LVOC class, while SVOC-class compounds are almost non-existent. This is also seen in the α-pinene reference experiment, where most of the compounds are attributed to a single VBS bin. Note also the different y scale in the α-pinene reference results compared to other results. A small number of signals in the sesquiterpene mixture results can confidently be categorized as thermal decomposition products, namely the ones that fall into the ELVOC volatility range but have relatively small molecular masses (< 200 Da). These compounds are C3–C7 compounds with relatively high oxygen content (O3–O7) and comprise about 11 % of the total integrated signal.

In the Scots pine results (Fig. 7), a similar shift from higher to lower volatilities can be seen, with Scots pine experiment 4 having the lowest volatility overall. Differences in the Scots pine VBSs are probably due to evolving VOC emissions from the sapling. Note that simple SQT / MT ratio calculated from the total concentration of monoterpenes and sesquiterpenes (Table 1; insets in Fig. 7, top row) cannot explain the change in the volatility.

Finally, we examine the compositional information present in the FIGAERO datasets. In Fig. 8, we plot the carbon numbers versus oxygen numbers for each compound for each experiment, coloured according to the T_{max}-derived saturation concentration (C^*). The panels reveal the spread of

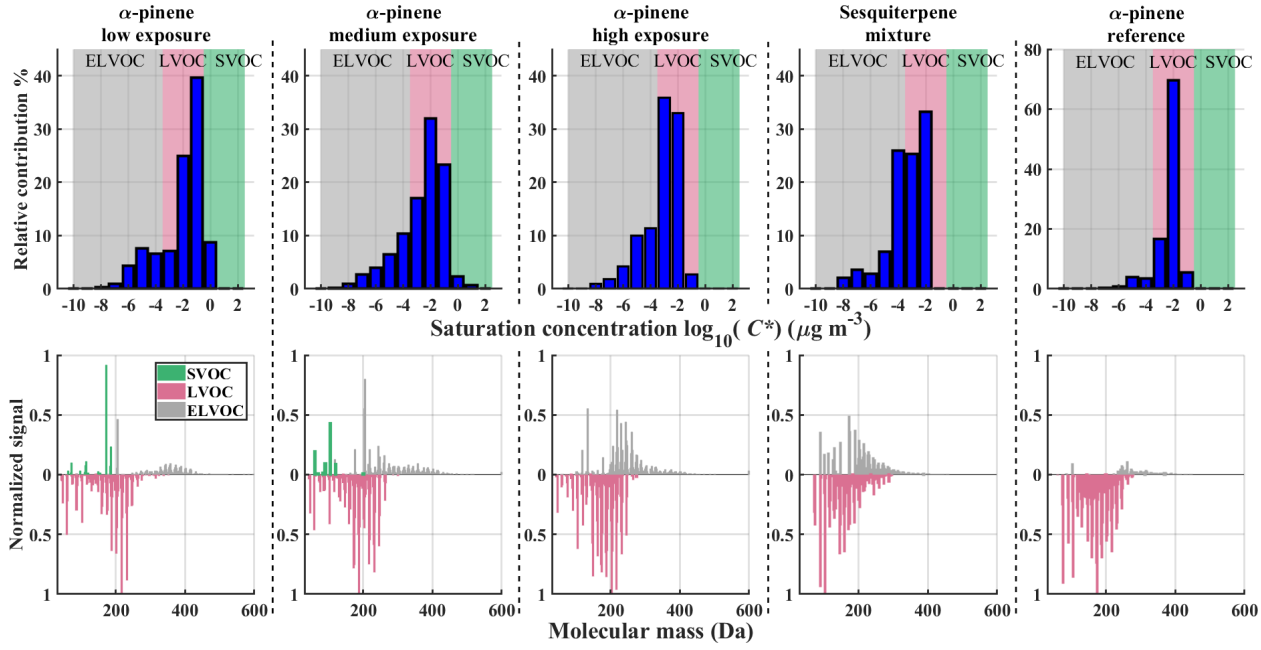

Figure 6. VBS bins and corresponding normalized integrated mass spectra from α-pinene low, medium and high experiment; sesquiterpene mixture; and α-pinene reference experiment. Top row: VBS bins determined from T_{max} with background colours corresponding to different volatility classes (defined in the text). Bottom row: integrated FIGAERO signal normalized to maximum signal and coloured by corresponding volatility class. LVOC-class compounds (red) are plotted on an inverted y axis to more easily distinguish them from other volatility classes.

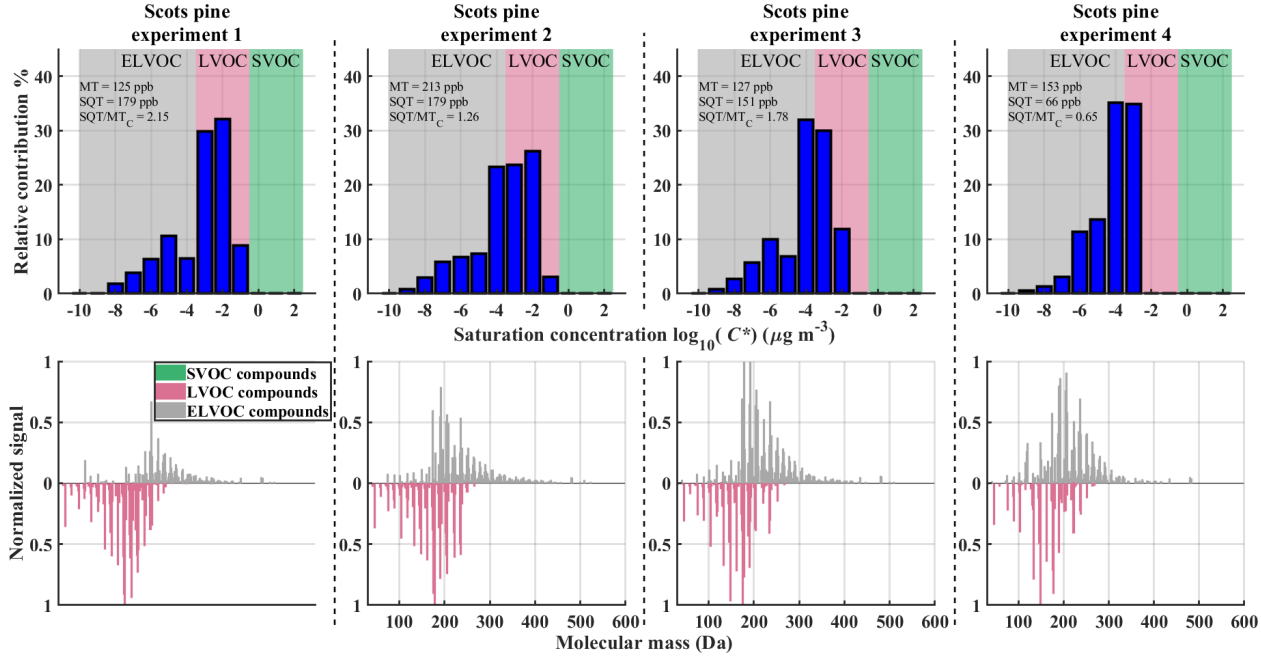

Figure 7. VBS bins and corresponding normalized integrated mass spectra in the Scots pine experiments. Top row: VBS bins determined from T_{max} with background colours corresponding to different volatility classes. Bottom row: integrated FIGAERO signal normalized to maximum signal coloured by corresponding volatility class. LVOC class is plotted on reverse y axis to more easily distinguish them from other volatility classes. Text in the upper row panels shows measured amounts of monoterpenes and sesquiterpenes and calculated SQT / MT ratio per mass ratio.

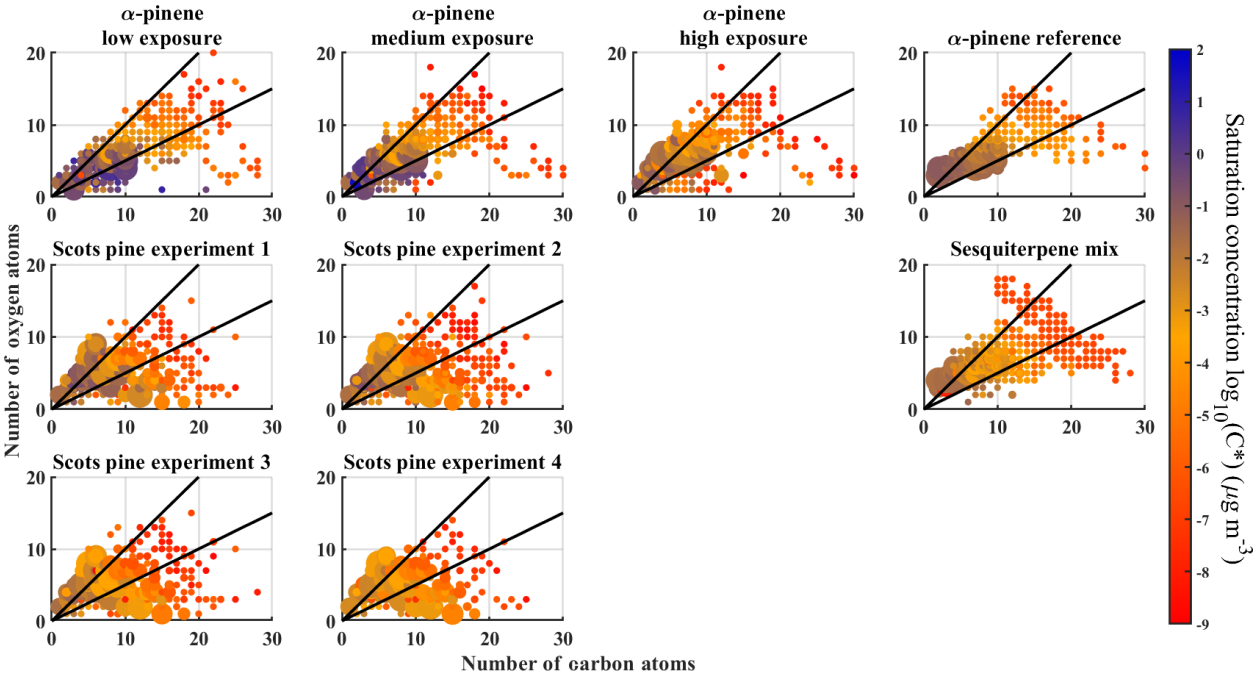

Figure 8. Number of oxygen molecules versus number of carbon molecules for each compound and each experiment. Colours correspond to the saturation ratio C^* as derived from the measured T_{max}. The size of a marker corresponds to the signal of the compound. The two black lines in the figures correspond to O : C = 0.5 and O : C = 1 ratios, for reference.

compounds across the ranges of O : C ratios. In the α-pinene and sesquiterpene mixture experiments, the compounds fall roughly into similar areas (i.e. range of O : C ratios is 0.5–1.0), but in the Scots pine experiments the spread across different O : C ratios is notably wider. Specifically, there is an increased contribution of both relatively small (#C $\sim$ 5) but highly oxygenated compounds and larger (#C $>$ 10) though less oxygenated compounds (O : C $<$ 0.5), both with relatively low effective volatility. This suggests that the bulk O : C ratio is insufficient for comparing the expected properties of SOA particles generated from mixtures of different VOC precursors (e.g. MT and SQT; cf. average O : C and OS_C values with standard deviations in Table 3). Partially, the profoundly different spread of O : C ratios in the Scots pine experiment results might also be due to more extensive thermal fragmentation in the FIGAERO desorption process.

4 Summary and conclusions

In this study, we compared the physicochemical properties of SOA particles generated from combined ozonolysis and photo-oxidation of (1) α-pinene, (2) a complex mixture of VOCs emitted from Scots pine saplings, and (3) a mixture of farnesenes and bisabolenes which were observed to comprise a significant fraction of the Scots pine emissions. Our measurements examined the SOA mass yield, as well as the chemical composition and the thermal desorption properties of SOA particulate constituents to assess their volatility. In general, we found that all of these quantities or properties are substantially controlled by the oxidative strength, as expected, but crucially also by the identity of the isomers making up the precursor VOC mixture.

The SOA mass yield from Scots pine emissions was in general lower than the SOA yield from α-pinene. The notable exception is a single experiment (Scots pine experiment 4) in which plant emissions were not dominated by farnesene and sesquiterpenes with similar structure but by β-phellandrene and other monoterpenes. That experiment had the highest SOA yields among the Scots pine experiments, which is consistent with the high yields for the specifically involved monoterpenes reported or suggested in the literature (e.g. Faiola et al., 2018). For the other Scots pine experiments (experiments 1–3), we attribute the low observed SOA yields to the substantial contribution of acyclic sesquiterpenes, particularly β- and α-farnesene, to the total terpenoid plant emissions in those cases, ranging from 40 % to 70 % by mass. This is supported by our additional experiments that resulted in a much lower SOA yield from a mixture of monocyclic and acyclic sesquiterpenes than from α-pinene. The fragmentation of acyclic sesquiterpenes likely results in a product distribution containing a smaller amount of organic material with sufficiently low volatility to partition from the gas to particle phase. These acyclic sesquiterpenes might also go through multiple cycles of auto-oxidation following the reaction with OH, before suffering substantial fragmentation (Bianchi et al., 2019), which would explain the relatively

high (> 5) number of oxygen atoms in a major fraction of the products comprising SOA.

Indeed, our thermal desorption results indicate that the oxidation of acyclic and monocyclic sesquiterpenes forms a substantial number of relatively small compounds, compared to α-pinene (Fig. 4). The average molecular weight of particle-phase α-pinene oxidation products decreases with increasing OH exposure (Table 3), while their O : C ratio increases. At the same time, the thermal desorption temperature of the SOA particulate constituents increases (Figs. 5–6), indicating a decrease in the effective SOA particle volatility.

Interestingly, our measurements showed that our Scots pine and sesquiterpene SOA particles were of lower volatility than any of the α-pinene SOA particles (even at higher oxidation exposure and comparable O : C and OS_C values). This result is indicated by both sum thermograms and supported by their derived VBS distributions for the individual SOA particulate constituents. It is also worth noting that, for the Scots pine experiments, the lowest-volatility SOA is formed in the experiment resulting in the highest SOA yields (Scots pine experiment 4), contrary to the observations made for the α-pinene experiments.

The molecular composition and thermal desorption behaviour of SOA particles observed with the FIGAERO instruments in experiment 4 were strikingly similar to the other, sesquiterpene-dominated, Scots pine experiments 1–3. It appears that a certain contribution of those acyclic sesquiterpenes was sufficient to lower SOA volatility, whereas the monoterpenes that dominated the mixture led to the efficient formation of SOA to start with. Interestingly though, the monoterpenes did not seem to directly affect the volatility of Scots pine SOA, at least for our experiments here, even though their relative contribution to the precursor VOC mixture varied substantially. Further experiments are clearly warranted to explore this suggestion for a wider range of conditions and precursor mixtures than covered by this study.

In conclusion, our results highlight the need to know the structural identity of mixtures of VOCs, as typically encountered in real atmospheric conditions, if one endeavours to make an accurate prediction of SOA yields and SOA particle properties. In particular the emissions of sesquiterpenes need to be considered more carefully in current atmospheric models. Importantly, their effects on SOA yields can be both enhancing and suppressing, depending on the isomers involved. Specifically, depending on which sesquiterpene isomers are involved, the product distributions obtained from their oxidation can differ substantially from each other in terms of the products' volatility and of the subsequent SOA chemistry. At the very least, a differentiation between cyclic and acyclic terpenes is desirable. This issue is likely to become more relevant in the future, when biological and abiotic plant-stressed events increase in frequency as is projected for a warming climate (Bale et al., 2002; Jactel et al., 2019). Such stresses will both increase biogenic VOC emissions and change the composition of emitted mixtures (Faiola et al., 2018, 2019).

Data availability. The data shown in the paper are available on request from corresponding author and from Siegfried Schobesberger (siegfried.schobesberger@uef.fi).

Supplement. The supplement related to this article is available online at: https://doi.org/10.5194/acp-20-5629-2020-supplement.

Author contributions. AV, CF, AB and TYJ designed the study. AY, AB, ZL, LB, AL, CF, EK and SN performed the measurements. AY and SS led the paper writing, and all of the co-authors participated in the interpretation of the results and paper editing.

Competing interests. The authors declare that they have no conflict of interest.

Acknowledgements. The authors wish to thank James Blande, Minna Kivimäenpää and Rajendra Ghimire (University of Eastern Finland, Department of Environmental and Biological Sciences) for tending the Scots pine seedlings. Sergey A. Nizkorodov acknowledges the Fulbright Finland Foundation and the Saastamoinen Foundation for funding his visit to the University of Eastern Finland.

Financial support. his research was supported by the Academy of Finland (272041, 310682, 299544), European Research Council (ERC-StQ QAPPA 335478) and University of Eastern Finland Doctoral Program in Environmental Physics, Health and Biology.

Review statement. This paper was edited by Barbara Ervens and Jacqui Hamilton and reviewed by two anonymous referees.

References

Amin, H., Atkins, P. T., Russo, R. S., Brown, A. W., Sive, B., Hallar, A. G., and Huff Hartz, K. E.: Effect of Bark Beetle Infestation on Secondary Organic Aerosol Precursor Emissions, Environ. Sci. Technol., 46, 5696–5703, https://doi.org/10.1021/es204205m, 2012.

Bäck, J., Aalto, J., Henriksson, M., Hakola, H., He, Q., and Boy, M.: Chemodiversity of a Scots pine stand and implications for terpene air concentrations, Biogeosciences, 9, 689–702, https://doi.org/10.5194/bg-9-689-2012, 2012.

Bale, J. S., Masters, G. J., Hodkinson, I. A. N. D., Awmack, C., Bezemer, T. M., Brown, V. K., Butterfield, J., Buse, A., Coulson, J. C., Farrar, J., Good, J. E. G., Harrington, R., Hartley, S., Jones, T. H., Lindroth, R. L., and Press, M. C.: Herbivory in global climate change research: direct effects of rising temperature on insect herbivores, Glob. Chang. Biol., 8, 1–16, https://doi.org/10.1046/j.1365-2486.2002.00451.x, 2002.

Bannan, T. J., Le Breton, M., Priestley, M., Worrall, S. D., Bacak, A., Marsden, N. A., Mehra, A., Hammes, J., Hallquist, M., Al-

farra, M. R., Krieger, U. K., Reid, J. P., Jayne, J., Robinson, W., McFiggans, G., Coe, H., Percival, C. J., and Topping, D.: A method for extracting calibrated volatility information from the FIGAERO-HR-ToF-CIMS and its experimental application, Atmos. Meas. Tech., 12, 1429–1439, https://doi.org/10.5194/amt-12-1429-2019, 2019.

Berg, A. R., Heald, C. L., Huff Hartz, K. E., Hallar, A. G., Meddens, A. J. H., Hicke, J. A., Lamarque, J.-F., and Tilmes, S.: The impact of bark beetle infestations on monoterpene emissions and secondary organic aerosol formation in western North America, Atmos. Chem. Phys., 13, 3149–3161, https://doi.org/10.5194/acp-13-3149-2013, 2013.

Bianchi, F., Kurten, T., Riva, M., Mohr, C., Rissanen, M. P., Roldin, P., Berndt, T., Crounse, J. D., Wennberg, P. O., Mentel, T. F., Wildt, J., Junninen, H., Jokinen, T., Kulmala, M., Worsnop, D. R., Thornton, J. A., Donahue, N., Kjaergaard, H. G., and Ehn, M.: Highly Oxygenated Organic Molecules (HOM) from Gas-Phase Autoxidation Involving Peroxy Radicals: A Key Contributor to Atmospheric Aerosol, Chem. Rev., 119, 3472–3509, https://doi.org/10.1021/acs.chemrev.8b00395, 2019.

Blande, J. D., Turunen, K., and Holopainen, J. K.: Pine weevil feeding on Norway spruce bark has a stronger impact on needle VOC emissions than enhanced ultraviolet-B radiation, Environ. Pollut., 157, 174–180, https://doi.org/10.1016/J.ENVPOL.2008.07.007, 2009.

Buchholz, A., Lambe, A. T., Ylisirniö, A., Li, Z., Tikkanen, O.-P., Faiola, C., Kari, E., Hao, L., Luoma, O., Huang, W., Mohr, C., Worsnop, D. R., Nizkorodov, S. A., Yli-Juuti, T., Schobesberger, S., and Virtanen, A.: Insights into the O : C-dependent mechanisms controlling the evaporation of α-pinene secondary organic aerosol particles, Atmos. Chem. Phys., 19, 4061–4073, https://doi.org/10.5194/acp-19-4061-2019, 2019.

Capouet, M. and Müller, J.-F.: A group contribution method for estimating the vapour pressures of α-pinene oxidation products, Atmos. Chem. Phys., 6, 1455–1467, https://doi.org/10.5194/acp-6-1455-2006, 2006.

Donahue, N. M., Epstein, S. A., Pandis, S. N., and Robinson, A. L.: A two-dimensional volatility basis set: 1. organic-aerosol mixing thermodynamics, Atmos. Chem. Phys., 11, 3303–3318, https://doi.org/10.5194/acp-11-3303-2011, 2011.

Faiola, C. L., Buchholz, A., Kari, E., Yli-Pirilä, P., Holopainen, J. K., Kivimäenpää, M., Miettinen, P., Worsnop, D. R., Lehtinen, K. E. J., Guenther, A. B., and Virtanen, A.: Terpene Composition Complexity Controls Secondary Organic Aerosol Yields from Scots Pine Volatile Emissions, Sci. Rep., 8, 1–13, https://doi.org/10.1038/s41598-018-21045-1, 2018.

Faiola, C. L., Pullinen, I., Buchholz, A., Khalaj, F., Ylisirnio, A., Kari, E., Schobesberger, S., Yli-juuti, T., Miettinen, P., Holopainen, J. K., and Kivima, M.: Secondary Organic Aerosol Formation from Healthy and Aphid-Stressed Scots Pine Emissions, ACS Earth Space Chem., 3, 1756–1772, https://doi.org/10.1021/acsearthspacechem.9b00118, 2019.

Glasius, M. and Goldstein, A. H.: Recent Discoveries and Future Challenges in Atmospheric Organic Chemistry, Environ. Sci. Technol., 50, 2754–2764, https://doi.org/10.1021/acs.est.5b05105, 2016.

Hakola, H., Tarvainen, V., Praplan, A. P., Jaars, K., Hemmilä, M., Kulmala, M., Bäck, J., and Hellén, H.: Terpenoid and carbonyl emissions from Norway spruce in Finland during the growing season, Atmos. Chem. Phys., 17, 3357–3370, https://doi.org/10.5194/acp-17-3357-2017, 2017.

Hall, W. A., Pennington, M. R., and Johnston, M. V.: Molecular transformations accompanying the aging of laboratory secondary organic aerosol, Environ. Sci. Technol., 47, 2230–2237, https://doi.org/10.1021/es303891q, 2013.

Hallquist, M., Wenger, J. C., Baltensperger, U., Rudich, Y., Simpson, D., Claeys, M., Dommen, J., Donahue, N. M., George, C., Goldstein, A. H., Hamilton, J. F., Herrmann, H., Hoffmann, T., Iinuma, Y., Jang, M., Jenkin, M. E., Jimenez, J. L., Kiendler-Scharr, A., Maenhaut, W., McFiggans, G., Mentel, Th. F., Monod, A., Prévôt, A. S. H., Seinfeld, J. H., Surratt, J. D., Szmigielski, R., and Wildt, J.: The formation, properties and impact of secondary organic aerosol: current and emerging issues, Atmos. Chem. Phys., 9, 5155–5236, https://doi.org/10.5194/acp-9-5155-2009, 2009.

Hellén, H., Praplan, A. P., Tykkä, T., Ylivinkka, I., Vakkari, V., Bäck, J., Petäjä, T., Kulmala, M., and Hakola, H.: Long-term measurements of volatile organic compounds highlight the importance of sesquiterpenes for the atmospheric chemistry of a boreal forest, Atmos. Chem. Phys., 18, 13839–13863, https://doi.org/10.5194/acp-18-13839-2018, 2018.

Holopainen, J. K. and Gershenzon, J.: Multiple stress factors and the emission of plant VOCs, Trends Plant Sci., 15, 176–184, https://doi.org/10.1016/j.tplants.2010.01.006, 2010.

Holopainen, J. K., Kivimäenpää, M., and Nizkorodov, S. A.: Plant-derived Secondary Organic Material in the Air and Ecosystems, Trends Plant Sci., 22, 744–753, https://doi.org/10.1016/j.tplants.2017.07.004, 2017.

Huang, W., Saathoff, H., Pajunoja, A., Shen, X., Naumann, K.-H., Wagner, R., Virtanen, A., Leisner, T., and Mohr, C.: α-Pinene secondary organic aerosol at low temperature: chemical composition and implications for particle viscosity, Atmos. Chem. Phys., 18, 2883–2898, https://doi.org/10.5194/acp-18-2883-2018, 2018.

Iyer, S., He, X., Hyttinen, N., Kurtén, T., and Rissanen, M. P.: Computational and Experimental Investigation of the Detection of HO_2 Radical and the Products of Its Reaction with Cyclohexene Ozonolysis Derived RO_2 Radicals by an Iodide-Based Chemical Ionization Mass Spectrometer, J. Phys. Chem. A, 121, 6778–6789, https://doi.org/10.1021/acs.jpca.7b01588, 2017.

Jactel, H., Koricheva, J., and Castagneyrol, B.: ScienceDirect Responses of forest insect pests to climate change: not so simple, Curr. Opin. Insect Sci., 35, 103–108, https://doi.org/10.1016/j.cois.2019.07.010, 2019.

Jaoui, M., Leungsakul, S., and Kamens, R. M.: Gas and Particle Products Distribution from the Reaction of β-Caryophyllene with Ozone, J. Atmos. Chem., 45, 261–287, 261–287, 2003.

Jaoui, M., Kleindienst, T. E., Docherty, K. S., Lewandowski, M., and Offenberg, J. H.: Secondary organic aerosol formation from the oxidation of a series of sesquiterpenes: α-cedrene, β-caryophyllene, α-humulene and α-farnesene with O_3, OH and NO_3 radicals, Environ. Chem., 10, 178, https://doi.org/10.1071/EN13025, 2013.

Jaoui, M., Lewandowski, M., Offenberg, J. H., Docherty, K. S., and Kleindienst, T. E.: Ozonolysis of α/β-farnesene mixture: Analysis of gas-phase and particulate reaction products, Atmos. Environ., 169, 175–192, https://doi.org/10.1016/j.atmosenv.2017.08.065, 2017.

Jimenez, J. L., Canagaratna, M. R., Donahue, N. M., Prevot, A. S. H., Zhang, Q., Kroll, J. H., DeCarlo, P. F., Allan, J. D., Coe, H., Ng, N. L., Aiken, A. C., Docherty, K. S., Ulbrich, I. M., Grieshop, A. P., Robinson, A. L., Duplissy, J., Smith, J. D., Wilson, K. R., Lanz, V. A., Hueglin, C., Sun, Y. L., Tian, J., Laaksonen, A., Raatikainen, T., Rautiainen, J., Vaattovaara, P., Ehn, M., Kulmala, M., Tomlinson, J. M., Collins, D. R., Cubison, M. J., Dunlea, E. J., Huffman, J. A., Onasch, T. B., Alfarra, M. R., Williams, P. I., Bower, K., Kondo, Y., Schneider, J., Drewnick, F., Borrmann, S., Weimer, S., Demerjian, K., Salcedo, D., Cottrell, L., Griffin, R., Takami, A., Miyoshi, T., Hatakeyama, S., Shimono, A., Sun, J. Y., Zhang, Y. M., Dzepina, K., Kimmel, J. R., Sueper, D., Jayne, J. T., Herndon, S. C., Trimborn, A. M., Williams, L. R., Wood, E. C., Middlebrook, A. M., Kolb, C. E., Baltensperger, U., Worsnop, D. R., and Worsnop, D. R.: Evolution of organic aerosols in the atmosphere, Science, 326, 1525–1529, https://doi.org/10.1126/science.1180353, 2009.

Junninen, H., Ehn, M., Petäjä, T., Luosujärvi, L., Kotiaho, T., Kostiainen, R., Rohner, U., Gonin, M., Fuhrer, K., Kulmala, M., and Worsnop, D. R.: A high-resolution mass spectrometer to measure atmospheric ion composition, Atmos. Meas. Tech., 3, 1039–1053, https://doi.org/10.5194/amt-3-1039-2010, 2010.

Kang, E., Root, M. J., Toohey, D. W., and Brune, W. H.: Introducing the concept of Potential Aerosol Mass (PAM), Atmos. Chem. Phys., 7, 5727–5744, https://doi.org/10.5194/acp-7-5727-2007, 2007.

Kari, E., Miettinen, P., Yli-Pirilä, P., Virtanen, A., and Faiola, C. L.: PTR-ToF-MS product ion distributions and humidity-dependence of biogenic volatile organic compounds, Int. J. Mass Spectrom., 430, 87–97, https://doi.org/10.1016/j.ijms.2018.05.003, 2018.

Kim, D., Stevens, P. S., and Hites, R. A.: Rate constants for the gas-phase reactions of OH and O_3 with β-ocimene,β-myrcene, and α-and β-farnesene as a function of temperature, J. Phys. Chem. A, 115, 500–506, https://doi.org/10.1021/jp111173s, 2011.

Kourtchev, I., Bejan, I., Sodeau, J. R., and Wenger, J. C.: Gas-phase reaction of (E)-β-farnesene with ozone: Rate coefficient and carbonyl products, Atmos. Environ., 43, 3182–3190, https://doi.org/10.1016/j.atmosenv.2009.03.048, 2009.

Kourtchev, I., Bejan, I., Sodeau, J. R., and Wenger, J. C.: Gas phase reaction of OH radicals with (E)-β-farnesene at 296 $\pm$ 2 K: Rate coefficient and carbonyl products, Atmos. Environ., 46, 338–345, https://doi.org/10.1016/j.atmosenv.2011.09.061, 2012.

Krieger, U. K., Siegrist, F., Marcolli, C., Emanuelsson, E. U., Gøbel, F. M., Bilde, M., Marsh, A., Reid, J. P., Huisman, A. J., Riipinen, I., Hyttinen, N., Myllys, N., Kurtén, T., Bannan, T., Percival, C. J., and Topping, D.: A reference data set for validating vapor pressure measurement techniques: homologous series of polyethylene glycols, Atmos. Meas. Tech., 11, 49–63, https://doi.org/10.5194/amt-11-49-2018, 2018.

Kroll, J. H., Donahue, N. M., Jimenez, J. L., Kessler, S. H., Canagaratna, M. R., Wilson, K. R., Altieri, K. E., Mazzoleni, L. R., Wozniak, A. S., Bluhm, H., Mysak, E. R., Smith, J. D., Kolb, C. E., and Worsnop, D. R.: Carbon oxidation state as a metric for describing the chemistry of atmospheric organic aerosol, Nat. Chem., 3, 133–139, https://doi.org/10.1038/nchem.948, 2011.

Lambe, A. T., Ahern, A. T., Williams, L. R., Slowik, J. G., Wong, J. P. S., Abbatt, J. P. D., Brune, W. H., Ng, N. L., Wright, J. P., Croasdale, D. R., Worsnop, D. R., Davidovits, P., and Onasch, T. B.: Characterization of aerosol photooxidation flow reactors: heterogeneous oxidation, secondary organic aerosol formation and cloud condensation nuclei activity measurements, Atmos. Meas. Tech., 4, 445–461, https://doi.org/10.5194/amt-4-445-2011, 2011.

Lambe, A. T., Onasch, T. B., Croasdale, D. R., Wright, J. P., Martin, A. T., Franklin, J. P., Massoli, P., Kroll, J. H., Canagaratna, M. R., Brune, W. H., Worsnop, D. R., and Davidovits, P.: Transitions from Functionalization to Fragmentation Reactions of Laboratory Secondary Organic Aerosol (SOA) Generated from the OH Oxidation of Alkane Precursors, Environ. Sci. Technol., 46, 5430–5437, https://doi.org/10.1021/es300274t, 2012.

Lee, A., Goldstein, A. H., Kroll, J. H., Ng, N. L., Varutbangkul, V., Flagan, R. C., and Seinfeld, J. H.: Gas-phase products and secondary aerosol yields from the photooxidation of 16 different terpenes, J. Geophys. Res., 111, D17305, https://doi.org/10.1029/2006JD007050, 2006.

Lee, B. H., Lopez-Hilfiker, F. D., Mohr, C., Kurtén, T., Worsnop, D. R., and Thornton, J. A.: An Iodide-Adduct High-Resolution Time-of-Flight Chemical-Ionization Mass Spectrometer: Application to Atmospheric Inorganic and Organic Compounds, Environ. Sci. Technol., 48, 6309–6317, https://doi.org/10.1021/es500362a, 2014.

Lopez-Hilfiker, F. D., Mohr, C., Ehn, M., Rubach, F., Kleist, E., Wildt, J., Mentel, Th. F., Lutz, A., Hallquist, M., Worsnop, D., and Thornton, J. A.: A novel method for online analysis of gas and particle composition: description and evaluation of a Filter Inlet for Gases and AEROsols (FIGAERO), Atmos. Meas. Tech., 7, 983–1001, https://doi.org/10.5194/amt-7-983-2014, 2014.

Lopez-Hilfiker, F. D., Mohr, C., Ehn, M., Rubach, F., Kleist, E., Wildt, J., Mentel, Th. F., Carrasquillo, A. J., Daumit, K. E., Hunter, J. F., Kroll, J. H., Worsnop, D. R., and Thornton, J. A.: Phase partitioning and volatility of secondary organic aerosol components formed from α-pinene ozonolysis and OH oxidation: the importance of accretion products and other low volatility compounds, Atmos. Chem. Phys., 15, 7765–7776, https://doi.org/10.5194/acp-15-7765-2015, 2015.

Mackenzie-Rae, F. A., Liu, T., Deng, W., Saunders, S. M., Fang, Z., Zhang, Y., and Wang, X.: Ozonolysis of α-phellandrene – Part 1: Gas- and particle-phase characterisation, Atmos. Chem. Phys., 17, 6583–6609, https://doi.org/10.5194/acp-17-6583-2017, 2017.

McFiggans, G., Mentel, T. F., Wildt, J., Pullinen, I., Kang, S., Kleist, E., Schmitt, S., Springer, M., Tillmann, R., Wu, C., Zhao, D., Hallquist, M., Faxon, C., Breton, M. Le, Hallquist, A. M., Simpson, D., Bergstro, R., Jenkin, M. E., Ehn, M., Thornton, J. A., Alfarra, M. R., Bannan, T. J., Percival, C. J., Priestley, M., Topping, D., and Kiendler-scharr, A.: Secondary organic aerosol reduced by mixture of atmospheric vapours, Nature, 565, 587–593, https://doi.org/10.1038/s41586-018-0871-y, 2019.

Ng, N. L., Brown, S. S., Archibald, A. T., Atlas, E., Cohen, R. C., Crowley, J. N., Day, D. A., Donahue, N. M., Fry, J. L., Fuchs, H., Griffin, R. J., Guzman, M. I., Herrmann, H., Hodzic, A., Iinuma, Y., Jimenez, J. L., Kiendler-Scharr, A., Lee, B. H., Luecken, D. J., Mao, J., McLaren, R., Mutzel, A., Osthoff, H. D., Ouyang, B., Picquet-Varrault, B., Platt, U., Pye, H. O. T., Rudich, Y., Schwantes, R. H., Shiraiwa, M., Stutz, J., Thornton, J. A., Tilgner, A., Williams, B. J., and Zaveri, R. A.: Nitrate radicals and biogenic volatile organic compounds: oxidation, mecha-

nisms, and organic aerosol, Atmos. Chem. Phys., 17, 2103–2162, https://doi.org/10.5194/acp-17-2103-2017, 2017.

Odum, J. R., Hoffmann, T., Bowman, F., Collins, D., Flagan Richard, C., and Seinfeld, J. H.: Gas particle partitioning and secondary organic aerosol yields, Environ. Sci. Technol., 30, 2580–2585, https://doi.org/10.1021/es950943+, 1996.

Palm, B. B., Campuzano-Jost, P., Ortega, A. M., Day, D. A., Kaser, L., Jud, W., Karl, T., Hansel, A., Hunter, J. F., Cross, E. S., Kroll, J. H., Peng, Z., Brune, W. H., and Jimenez, J. L.: In situ secondary organic aerosol formation from ambient pine forest air using an oxidation flow reactor, Atmos. Chem. Phys., 16, 2943–2970, https://doi.org/10.5194/acp-16-2943-2016, 2016.

Pankow, J. F.: An absorption model of the gas/aerosol partitioning involved in the formation of secondary organic aerosol, Atmos. Environ., 28, 189–193, https://doi.org/10.1016/1352-2310(94)90094-9, 1994.

Pankow, J. F. and Asher, W. E.: SIMPOL.1: a simple group contribution method for predicting vapor pressures and enthalpies of vaporization of multifunctional organic compounds, Atmos. Chem. Phys., 8, 2773–2796, https://doi.org/10.5194/acp-8-2773-2008, 2008.

Passananti, M., Zapadinsky, E., Zanca, T., Ehn, M., Attoui, M. and Vehkama, H.: ChemComm How well can we predict cluster fragmentation, Chem. Commun., 55, 5946–5949, https://doi.org/10.1039/c9cc02896j, 2019.

Peng, Z., Day, D. A., Stark, H., Li, R., Lee-Taylor, J., Palm, B. B., Brune, W. H., and Jimenez, J. L.: HO_x radical chemistry in oxidation flow reactors with low-pressure mercury lamps systematically examined by modeling, Atmos. Meas. Tech., 8, 4863–4890, https://doi.org/10.5194/amt-8-4863-2015, 2015.

Peng, Z., Day, D. A., Ortega, A. M., Palm, B. B., Hu, W., Stark, H., Li, R., Tsigaridis, K., Brune, W. H., and Jimenez, J. L.: Non-OH chemistry in oxidation flow reactors for the study of atmospheric chemistry systematically examined by modeling, Atmos. Chem. Phys., 16, 4283–4305, https://doi.org/10.5194/acp-16-4283-2016, 2016.

Riipinen, I., Yli-Juuti, T., Pierce, J. R., Petäjä, T., Worsnop, D. R., Kulmala, M. and Donahue, N. M.: The contribution of organics to atmospheric nanoparticle growth, Nat. Geosci., 5, 453–458, https://doi.org/10.1038/ngeo1499, 2012.

Schobesberger, S., D'Ambro, E. L., Lopez-Hilfiker, F. D., Mohr, C., and Thornton, J. A.: A model framework to retrieve thermodynamic and kinetic properties of organic aerosol from composition-resolved thermal desorption measurements, Atmos. Chem. Phys., 18, 14757–14785, https://doi.org/10.5194/acp-18-14757-2018, 2018.

Spanke, J., Rannik, Ü., Forkel, R., Nigge, W., and Hoffman, T.: Emission fluxes and atmospheric degradation of monoterpenes above a boreal forest: field measurements and modelling, Tellus B, 53, 406–422, https://doi.org/10.3402/tellusb.v53i4.16614, 2001.

Surratt, J. D., Goìmez-Gonzaìlez, Y., Chan, A. W. H., Vermeylen, R., Shahgholi, M., Kleindienst, T. E., Edney, E. O., Offenberg, J. H., Lewandowski, M., Jaoui, M., Maenhaut, W., Claeys, M., Flagan, R. C., and Seinfeld, J. H.: Organosulfate Formation in Biogenic Secondary Organic Aerosol, J. Phys. Chem. A, 112, 8345–8378, https://doi.org/10.1021/jp802310p, 2008.

Yassaa, N., Song, W., Lelieveld, J., Vanhatalo, A., Bäck, J., and Williams, J.: Diel cycles of isoprenoids in the emissions of Norway spruce, four Scots pine chemotypes, and in Boreal forest ambient air during HUMPPA-COPEC-2010, Atmos. Chem. Phys., 12, 7215–7229, https://doi.org/10.5194/acp-12-7215-2012, 2012.